ACS APPLIED MATERIALS & INTERFACES

Research Article

www.acsami.org

Superior Dehydrogenation/Hydrogenation Kinetics and Long-Term Cycling Performance of K and Rb Cocatalyzed $Mg(NH_2)_2$-2LiH system

Chao Li, Yongfeng Liu,* Ruijun Ma, Xin Zhang, You Li, Mingxia Gao, and Hongge Pan

State Key Laboratory of Silicon Materials, Key Laboratory of Advanced Materials and Applications for Batteries of Zhejiang Province, and Department of Materials Science and Engineering, Zhejiang University, Hangzhou 310027, China

Supporting Information

ABSTRACT: The coaddition of KH and RbH significantly improves the hydrogen storage properties of the $Mg(NH_2)_2$-2LiH system. An $Mg(NH_2)_2$-2LiH-0.04KH-0.04RbH composite was able to reversibly store 5.2 wt % H_2 when the dehydrogenation operates at 130 °C and the hydrogenation operates at 120 °C. The isothermal dehydrogenation rate at 130 °C was approximately 43 times that of a pristine sample. During ball-milling, KH reacts with RbH to form a K(Rb)H solid solution. Upon heating, RbH first separates from the K(Rb)H solid solution and participates in the first step of dehydrogenation reaction, and then the remaining KH participates in the second dehydrogenation reaction. The presence of RbH and KH provide synergetic effects, which improve the thermodynamics and kinetics of hydrogen storage in the $Mg(NH_2)_2$-2LiH system. In particular, more than 93% of the hydrogen storage capacity (4.4 wt %) remains after cycling a sample with 0.04 mol of KH and RbH for 50 cycles, indicating notably better cycling stability compared with any presently known Li−Mg−N−H systems.

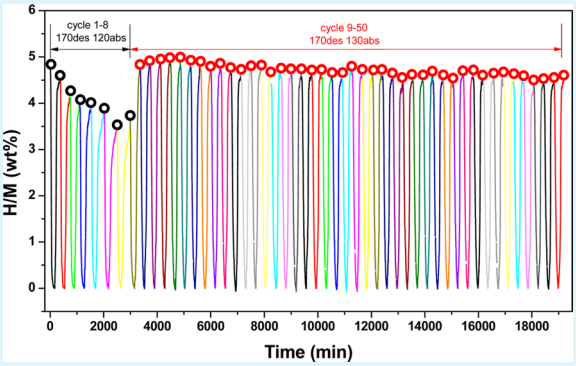

KEYWORDS: *hydrogen storage materials, amides, potassium hydride, rubidium hydride, cycling stability*

1. INTRODUCTION

Hydrogen is widely considered to be an ideal fuel for vehicular applications.[1] However, storing hydrogen in a safe, efficient, and economical manner remains a critical challenge for practical applications.[1−5] Solid-state hydrogen storage has considerable advantages compared with gaseous and liquid hydrogen storage in terms of safety and economy, but none of the solid-state hydrogen storage materials reported to date meet all of the on-board criteria.[6] There are still some materials with the potential to reach these standards, including alanates, borohydrides and metal−N−H systems.[7−12] It has previously been shown that approximately 5.6 wt % hydrogen can be reversibly stored in the $Mg(NH_2)_2$-2LiH system through the following reaction[11]

$$Mg(NH_2)_2 + 2LiH \leftrightarrow Li_2MgN_2H_2 + 2H_2 \quad (1)$$

However, the hydrogen release from reaction 1 at an appropriate rate can only proceed at temperatures above 200 °C, although the thermodynamically predicated operating temperature is approximately 90 °C at an equilibrium hydrogen pressure of 1 bar.[13,14] Considerable efforts have been devoted to lowering the operating temperature and enhancing the dehydrogenation kinetics of $Mg(NH_2)_2$-2LiH by reducing the particle size and doping with additives.[14−30] Xie et al. found that hydrogen desorption/absorption kinetics are distinctly increased by mixing smaller-sized $Mg(NH_2)_2$ with LiH.[15] $Li_2MgN_2H_2$ with a particle size of 100−200 nm has been shown to begin absorbing hydrogen at only 80 °C, approximately 100 °C lower than samples greater than 800 nm in size.[16] Alternatively, doping with additives is another important method for improving the hydrogen storage properties of the $Mg(NH_2)_2$-2LiH system. To date, five types of effective additives have been developed, including $Li_2MgN_2H_2$ seeds, carbon-based materials, transition metals and their compounds, metal borohydrides, and alkali-metal compounds.[14,17−30] Among these known materials, metal borohydrides and alkali-metal compounds are two of the most effective additives. Hu et al. demonstrated improvements in the dehydrogenation/hydrogenation kinetics and thermodynamics of the $Mg(NH_2)_2$-2LiH system by adding 0.1 mol of $LiBH_4$.[21] The introduction of $ZrCoH_3$ further improved the hydrogen storage properties of the $LiBH_4$-doped $Mg(NH_2)_2$-2LiH system.[22] In addition, it was recently found that a $Mg(NH_2)_2$-2LiH-0.1$Ca(BH_4)_2$ sample could reversibly release/take up 4 wt % H_2 below 140 °C because of the concerted effects of $LiBH_4$ and CaH_2 formed in situ during ball milling.[23] More encouragingly, the hydrogen storage properties of $Mg(NH_2)_2$-2LiH were significantly enhanced by introducing a small amount of KH.[25−28] Compared with an $Mg(NH_2)_2$-2LiH sample, the peak dehydrogenation temperature of an $Mg(NH_2)_2$-1.9LiH-0.1KH sample was lowered from 186 to 132 °C, and reversible hydrogen storage was possible in the PCT model at

Received: July 16, 2014
Accepted: September 9, 2014
Published: September 17, 2014

temperatures as low as 107 °C.[25] The superb effects of KH modification were further confirmed in studies that followed.[26−28] Our recent investigations revealed that a dehydrogenated $Mg(NH_2)_2$-2LiH-0.08KH sample can be fully hydrogenated at 140 °C.[28] Similar to K, Rb-based compounds are another efficient alkali-metal modifier.[29,30] The hydrogen storage thermodynamics and kinetics of the $Mg(NH_2)_2$-2LiH system were significantly improved by adding RbF, and the active species was identified to be RbH.[29,30] In particular, after being fully dehydrogenated at 130 °C, a $Mg(NH_2)_2$-2LiH-0.08RbF sample was fully hydrogenated at 120 °C, representing a 20 °C reduction relative to a sample modified with 0.08KH.[28,29] However, the hydrogen storage capacity was also decreased to approximately 4.8 wt % after adding 0.08 mol of RbF due to the larger molecular weight of RbF. In summary, both KH and RbH have been shown to significantly improve the hydrogen storage properties of the $Mg(NH_2)_2$-2LiH system. More importantly, RbH has been shown to be more effective for improving the hydrogenation properties of the $Mg(NH_2)_2$-2LiH system, but the hydrogen capacity of the Rb-modified $Mg(NH_2)_2$-2LiH system was distinctly reduced because of the larger molecular weight of Rb.

In this work, KH and RbH were simultaneously introduced into the $Mg(NH_2)_2$-2LiH system to achieve better hydrogen storage performance. As reported in our previous works, the total amount of KH and RbH added was optimized at 0.08 mol per mol of $Mg(NH_2)_2$-2LiH.[28,29] Accordingly, the KH and RbH coadded samples were obtained by partially replacing KH with RbH in the $Mg(NH_2)_2$-2LiH-0.08KH formulation. Five samples with compositions of $Mg(NH_2)_2$-2LiH-(0.08-x)KH-xRbH (x = 0, 0.02, 0.04, 0.06, 0.08) were prepared by ball milling the corresponding chemicals under 50 bar of H_2, and their dehydrogenation/hydrogenation behaviors were investigated systematically. The results showed that the hydrogen storage properties of $Mg(NH_2)_2$-2LiH-0.08KH were further improved by the presence of RbH. The $Mg(NH_2)_2$-2LiH-0.04KH-0.04RbH sample possessed the optimal hydrogen storage properties and could reversibly store 5.2 wt % H_2, where the dehydrogenation operated at 130 °C and the hydrogenation operated at 120 °C.

2. EXPERIMENTAL SECTION

The commercial chemicals, LiH (purity 98%) and KH (in mineral oil) were purchased from Alfa-Aesar. LiH was used as received, and KH was used after removing the mineral oil. $Mg(NH_2)_2$ was produced in-house by directly reacting Mg powder (99%, Sinopharm) with 7 bar of NH_3 at 300 °C. RbH was also synthesized in our laboratory by ball milling metallic Rb (99.75%, Alfa-Aesar) under 50 bar of H_2 at 500 rpm for 12 h. Prior to ball-milling, the milling vessel was first heated to 50 °C using a water bath and then wrapped with gauze for heat protection. Samples with compositions of $Mg(NH_2)_2$-2LiH-(0.08-x)KH-xRbH (x = 0, 0.02, 0.04, 0.06, 0.08) were prepared by ball milling the corresponding chemicals at 500 rpm on a planetary ball mill (QM-3SP4, Nanjing) for 36 h. The milling vessels were filled with 50 bar of hydrogen pressure to prevent hydrogen release during ball milling. All of the samples were handled in a MBRAUN glovebox filled with high purity argon to prevent contamination with air and moisture (O_2: < 1 ppm, H_2O: < 1 ppm).

Experiments investigating the temperature-dependence of hydrogen desorption were performed on a homemade temperature-programmed desorption (TPD) system coupled with a QIC-20 mass spectrometer (Hiden, England), which simultaneously recorded hydrogen (m/z: 2) and ammonia (m/z: 15). Approximately 50 mg of the sample was loaded and tested each time. Pure Ar was sent through the sample as the carrier gas in the testing process, and the sample was gradually heated to the preset temperature at a ramping rate of 2 °C/min. The dehydrogenation/hydrogenation quantities were determined using the volumetric method on a homemade Sieverts-type apparatus. Both isothermal and nonisothermal approaches were adopted, and approximately 120 mg sample was used for each experiment. In nonisothermal experiments, the temperature was gradually elevated at a rate of 2 °C/min for dehydrogenation and 1 °C/min for hydrogenation. For isothermal examination, the samples were quickly heated to and kept at a given temperature during the entire measurement. The sample temperature was measured and controlled with an automatic temperature controller and a thermocouple that was inserted into the sample interior. The reactor was evacuated prior to making measurements. For dehydrogenation, the gas was desorbed into a calibrated volume initially at 1×10^{-3} Torr, and the pressure increase was ~0.5 bar after the hydrogen desorption finished. For hydrogenation, the starting hydrogen pressure was 105 bar and the pressure above the sample was held above 105 bar because of the temperature effects during the course of the experiment. Differential scanning calorimetry (DSC) measurements were conducted on a Netzsch DSC 200 F3 unit. Approximately 5 mg of the sample was gradually heated up from room temperature to 300 °C at a rate of 2 °C/min under a flow of pure Ar.

The phase structures were characterized using an X'Pert PRO (PANalytical, The Netherlands) X-ray diffractometer using Cu Kα radiation at 40 kV and 40 mA. The XRD data were collected over the 2θ range of 10 to 90° with step increments of 0.05°. A homemade container was used to prevent the samples from contacting air and moisture during sample transfer and testing. N−H vibrations in all of the samples were identified on a Bruker Tensor 27 Fourier transform infrared spectrometer (Germany) operated in transmission mode. The test samples were prepared by cold pressing a mixture of powder samples and potassium bromide (KBr) powder at a 1:30 weight ratio to form a pellet. Each spectrum was created using an average of 16 scans with a 4 cm^{-1} resolution. The distribution of elemental Mg, K and Rb in the samples was analyzed using an energy-dispersive X-ray spectrometer (EDS) attached to a Hitachi S3700N scanning electron microscope (SEM).

X-ray photoelectron spectroscopy (XPS) analyses were conducted on a Kratos AXIS Ultra DLD spectrometer. The powder sample was pressed into a pellet at room temperature and adhered to the sample holder with double-sided carbon conductive tape. The sample was transferred from the glovebox to the XPS facility using a transfer vessel without exposing it to air. The XPS spectra were recorded using a monochromatic Al Kα (1486.6 eV) X-ray source under an ultimate pressure of 6.8×10^{-9} Torr. All data were calibrated using the adventitious C 1s signal at 284.8 eV as a reference.

3. RESULTS AND DISCUSSION

3.1. Compositional Dependence of Dehydrogenation/Hydrogenation Behaviors of $Mg(NH_2)_2$-2LiH-(0.08-x)KH-xRbH.

As previously reported, the amounts of K- and Rb-based additives were optimized at 0.08 mol in $Mg(NH_2)_2$-2LiH-xKH and $Mg(NH_2)_2$-2LiH-xRbF.[28,29] Therefore, we took the $Mg(NH_2)_2$-2LiH-0.08KH sample as a reference to design the KH and RbH comodified samples by partially replacing KH with RbH. Five $Mg(NH_2)_2$-2LiH-(0.08-x)KH-xRbH samples with x = 0, 0.02, 0.04, 0.06, and 0.08 were prepared by ball milling the corresponding chemicals under 50 bar of H_2. The as-prepared samples were subjected to structure and property evaluation. Figure 1 shows the TPD-MS curves of the as-prepared $Mg(NH_2)_2$-2LiH and $Mg(NH_2)_2$-2LiH-(0.08-x)KH-xRbH samples. The presence of KH and RbH significantly reduced the operating temperatures for hydrogen desorption compared with the $Mg(NH_2)_2$-2LiH system. Hydrogen desorption from the pristine $Mg(NH_2)_2$-2LiH sample began at 130 °C and terminated at 260 °C, with a distinct peak at 181 °C. After adding a small amount of KH and RbH, the onset

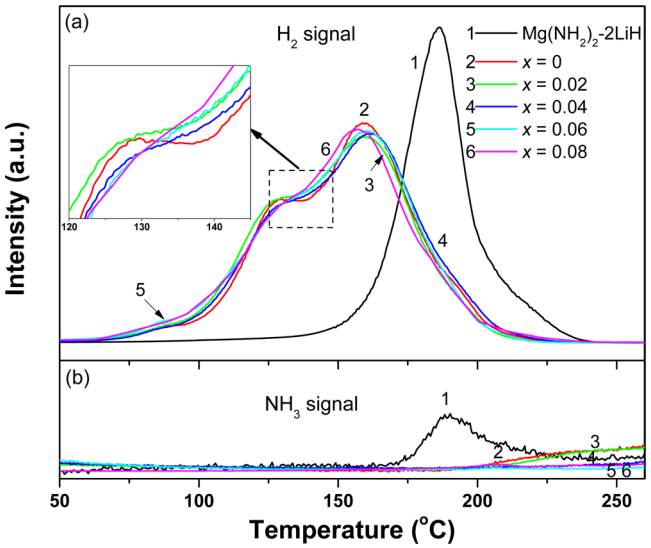

Figure 1. TPD-MS curves of $Mg(NH_2)_2$-2LiH and $Mg(NH_2)_2$-2LiH-(0.08-x)KH-xRbH samples milled for 36 h. (a) H_2 signal. (b) NH_3 signal.

temperature for hydrogen desorption was only 75 °C, representing a 55 °C reduction compared with the pristine $Mg(NH_2)_2$-2LiH sample. With increasing temperature, a shoulder at 130 °C and a distinct peak at 160 °C appeared, one after the other, suggesting a change in the dehydrogenation process. The dehydrogenation terminated at 220 °C for the samples with KH and RbH. At first glance, all of the KH- and RbH-modified samples exhibited very similar H_2 signal curves as a function of temperature. However, a closer examination revealed that there were some subtle differences among them. As shown in the inset of Figure 1a, the H_2 signal curves shifted slightly to lower temperatures with the addition of RbH, and slight overlapping was observed between the dehydrogenation shoulder and the main dehydrogenation peak, especially for the sample with x = 0.08. This phenomenon suggests that the added RbH participates in the first step of dehydrogenation.[29] Further MS examination showed that no NH_3 signal was detected for the KH and RbH-modified samples below 200 °C, indicating that the addition of KH and RbH significantly suppressed the evolution of NH_3 during the initial dehydrogenation process. When the sample temperature was higher than 200 °C, trace NH_3 was detected in the KH-modified samples. With the addition of RbH, the NH_3 evolution was gradually suppressed and even disappeared at x = 0.06 and 0.08. Clearly, RbH helps decrease the evolution of the NH_3 side product.

Further quantitative hydrogen desorption measurements were conducted using the volumetric method. The results are presented in Figure 2. The KH- and RbH-modified samples exhibited significantly reduced operating temperatures for hydrogen desorption compared with the pristine $Mg(NH_2)_2$-2LiH sample. In nonisothermal mode (Figure 2a), apparent hydrogen desorption was observed at 75 °C for the samples with KH and RbH, and hydrogen desorption finished at 220 °C, representing 55 and 40 °C reductions, respectively, compared with the pristine sample. When the amount of RbH added was increased from 0 to 0.08 mol, however, the dehydrogenation amount was slightly reduced from 5.3 to 5.0 wt % because of the larger molecular weight of Rb (85.5) compared with Li (6.9), Mg (24.3) and K (39.1). Furthermore, isothermal examination showed superior dehydrogenation kinetics for the KH and RbH-modified samples (Figure 2b). More than 3.5 wt % H_2, corresponding to 70% of the capacity, could be rapidly released from the $Mg(NH_2)_2$-2LiH-(0.08-x)KH-xRbH samples within 150 min at 130 °C. However, the pristine $Mg(NH_2)_2$-2LiH sample liberated only 0.5 wt % H_2 under the same conditions. From analysis of the tangent slope of the linear regions of the isothermal dehydrogenation curves, the rate constant for the sample with 0.04 mol of KH and RbH was determined to be 0.257 wt %/min, which is approximately 43 times greater than that of the pristine sample (0.006 wt %/min), indicating superior dehydrogenation kinetics caused by the presence of RbH. In addition, it should be noted that the amount of hydrogen desorption from the $Mg(NH_2)_2$-2LiH-0.08KH sample was 4.0 wt % within 360 min, while it was decreased to 3.76 wt % for the $Mg(NH_2)_2$-2LiH-0.08RbH sample. Again, these results confirm that increasing the amount of RbH slightly reduces the dehydrogenation capacity.

To evaluate the effects of KH and RbH on the hydrogenation properties, we first fully dehydrogenated $Mg(NH_2)_2$-2LiH-

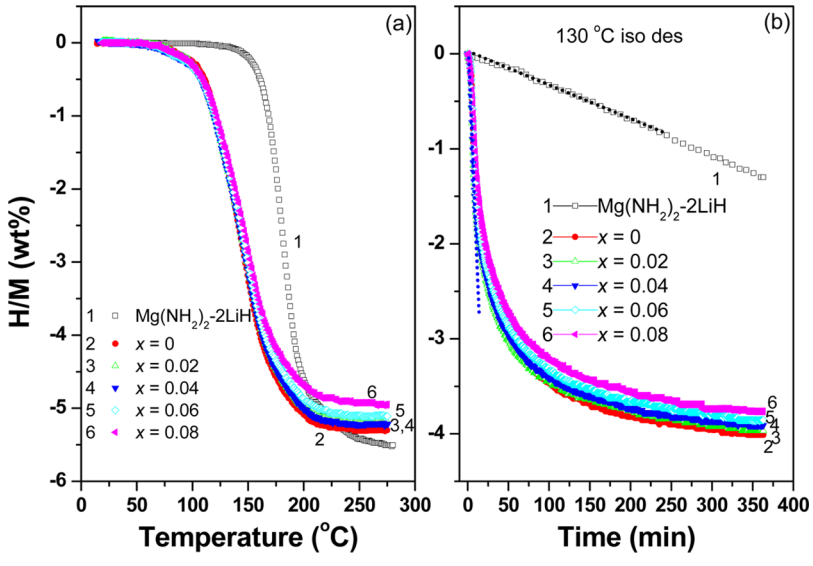

Figure 2. Nonisothermal (a) and isothermal (b) dehydrogenation curves of $Mg(NH_2)_2$-2LiH and $Mg(NH_2)_2$-2LiH-(0.08-x)KH-xRbH samples.

(0.08-x)KH-xRbH samples at 130 °C and then hydrogenated them at 105 bar H_2 in both nonisothermal and isothermal modes. Figure 3a shows the hydrogenation curves of the

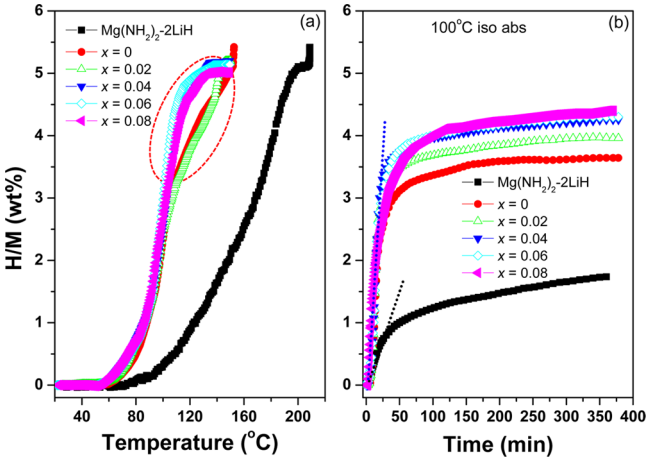

Figure 3. (a) Nonisothermal and (b) isothermal hydrogenation curves of $Mg(NH_2)_2$-2LiH and $Mg(NH_2)_2$-2LiH-(0.08-x)KH-xRbH samples.

$Mg(NH_2)_2$-2LiH-(0.08-x)KH-xRbH samples as a function of temperature. It can be observed that the hydrogen uptake of the dehydrogenated $Mg(NH_2)_2$-2LiH sample started at 80 °C and finished at 210 °C, with a total amount of 5.4 wt %. Interestingly, the onset temperature for hydrogen uptake in the KH- and RbH-modified samples was only 60 °C, and full hydrogenation was achieved at 130−150 °C. The amounts of hydrogen uptake were 5.3, 5.25, 5.2, 5.15, and 5.0 wt % for the samples with x = 0, 0.02, 0.04, 0.06, and 0.08, respectively, confirming a gradual decrease in the available hydrogen capacity because of the larger molecular weight of Rb as mentioned above. The ending temperature for hydrogen uptake was reduced by 60 °C at least from that of the pristine sample. In particular, faster kinetics were observed for the samples with x = 0.04, 0.06, and 0.08 than for those with x = 0 and 0.02 when the sample temperature was higher than 100 °C (Figure 3a). The isothermal hydrogenation experiments provided more obvious evidence for the accelerated absorption kinetics of the KH and RH-modified samples, especially for the samples with RbH. As shown in Figure 3b, the dehydrogenated $Mg(NH_2)_2$-2LiH-0.08KH sample took up approximately 3.4 wt % of hydrogen within 100 min at 100 °C, while only 1.2 wt % H_2 was recharged into the dehydrogenated pristine sample under the same conditions. Importantly, a further increase in the hydrogen uptake was found with increasing amounts of RbH. The hydrogen uptake was increased to 4.25 wt % for the $Mg(NH_2)_2$-2LiH-0.04KH-0.04RbH sample, and an additional 0.05 and 0.1 wt % of hydrogen were absorbed by the samples with x = 0.06 and 0.08 under the same condition. These results indicate that the presence of RbH further improved the hydrogenation kinetics. However, it should be noted that while dwelling at 100 °C for 360 min, the amount of hydrogen uptake was still lower than the maximum hydrogen capacity. Analysis of the tangent slope of the linear regions of the isothermal hydrogenation curves revealed a rate constant of 0.242 wt %/min for the sample with 0.04 mol KH and RbH, which was more than 6 times higher than that of the pristine sample (0.039 wt %/min). Furthermore, this hydrogenation rate was approximately 1.5 times higher than that of the sample with 0.08 mol KH, providing quantitative evidence for the improved hydrogenation kinetics caused by RbH.

On the basis of the above discussion, it was concluded that the coaddition of KH and RbH improved the hydrogenation kinetics of the $Mg(NH_2)_2$-2LiH-0.08KH system, but this coaddition was also associated with a gradual decrease in the hydrogen capacity. Considering both the hydrogen storage capacity and hydrogenation reaction kinetics, the coaddition of 0.04 mol KH and RbH appears to be the optimal combination. The $Mg(NH_2)_2$-2LiH-0.04KH-0.04RbH sample could reversibly store 5.2 wt % H_2 at near ambient temperatures (desorption operated at 130 °C and absorption operated at 120 °C). Moreover, hydrogen storage properties of the $Mg(NH_2)_2$-2LiH-0.04KH-0.04RbH sample are also superior to those of the $Mg(NH_2)_2$-2LiH-0.04RbH sample (see Figure S1 in the Supporting Information). Therefore, the following investigations of the hydrogen storage thermodynamics, reversibility and the corresponding mechanisms focus on the $Mg(NH_2)_2$-2LiH-0.04KH-0.04RbH formulation.

3.2. Dehydrogenation Thermodynamics and Kinetics of $Mg(NH_2)_2$-2LiH-0.04KH-0.04RbH. Figure 4a shows the DSC curves of $Mg(NH_2)_2$-2LiH, $Mg(NH_2)_2$-2LiH-0.08KH and

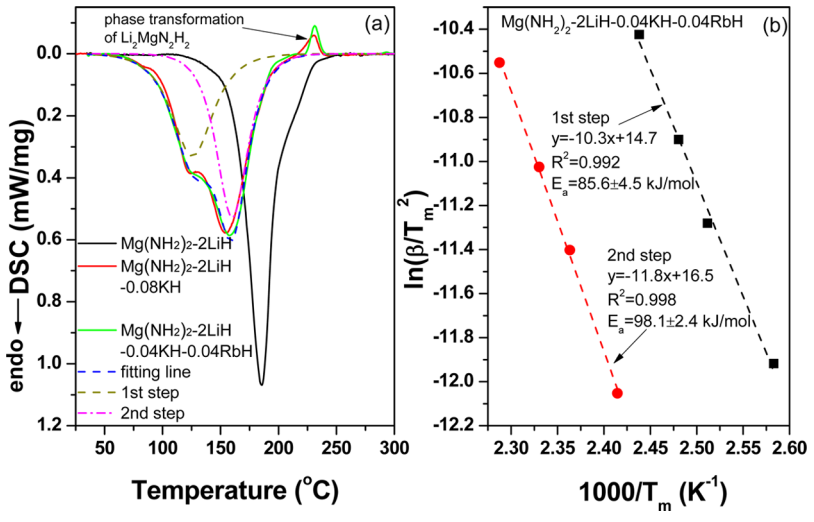

Figure 4. (a) DSC curves and (b) Kissinger's plots of $Mg(NH_2)_2$-2LiH, $Mg(NH_2)_2$-2LiH-0.08KH and $Mg(NH_2)_2$-2LiH-0.04KH-0.04RbH samples.

$Mg(NH_2)_2$-2LiH-0.04KH-0.04RbH. It can be observed that the $Mg(NH_2)_2$-2LiH-0.08KH and $Mg(NH_2)_2$-2LiH-0.04KH-0.04RbH samples exhibited nearly identical heat flow behavior. In the presence of KH and RbH, the endothermic peak significantly shifted to lower temperatures, and a new shoulder on the low-temperature side of the major endothermic peak appeared, suggesting a change in the dehydrogenation process. Moreover, an additional exothermic peak was also observed for the samples with KH and RbH at 220−250 °C. This exothermic peak can potentially be attributed to a polymorphic transformation of $Li_2MgN_2H_2$ from a cubic structure to an orthorhombic structure, as reported previously.[28,29] Integration of the endothermic peak revealed a heat effect of 1054 ± 10.5 J/g for the $Mg(NH_2)_2$-2LiH sample, which is equivalent to 39.4 ± 0.4 kJ/mol-H_2. For the $Mg(NH_2)_2$-2LiH-0.04KH-0.04RbH sample, the heat effects of the two dehydrogenation steps were estimated to be 443 ± 4.4 and 543 ± 5.4 J/g, corresponding to enthalpy changes of 38.1 ± 0.4 and 38.4 ± 0.4 kJ/mol-H_2, respectively, by fitting the DSC, TPD and volumetric release curves, which are slightly lower than that of the pristine sample. These results indicate that the presence of KH and RbH changed the reaction pathway of hydrogen desorption from the $Mg(NH_2)_2$-2LiH system and made it thermodynamically more favorable.

To quantitatively understand the effects of the coaddition of KH and RbH on the dehydrogenation kinetics, the apparent activation energy (E_a) was determined by the Kissinger's approach,[31] and the results are shown in Figure 4b. By fitting the data points, the values of E_a were calculated to be 85.6 ± 4.5 kJ/mol and 98.1 ± 2.4 kJ/mol for the first and second steps of dehydrogenation of $Mg(NH_2)_2$-2LiH-0.04KH-0.04RbH, representing a distinct reduction with respect to the pristine $Mg(NH_2)_2$-2LiH (103.9 ± 3.6 kJ/mol),[28] indicating that the coaddition of KH and RbH also reduces the kinetic barrier for hydrogen desorption from the $Mg(NH_2)_2$-2LiH system, which is another reason for the reduced dehydrogenation operating temperature. Interestingly, the E_a value of the first dehydrogenation step is almost identical to that of the $Mg(NH_2)_2$-2LiH-0.08KH sample (84.8 ± 3.5 kJ/mol), but that of the second dehydrogenation step is slightly lower than that of $Mg(NH_2)_2$-2LiH-0.08KH (103.0 ± 2.7 kJ/mol).[28] This fact indicates that the presence of RbH facilitates the further reduction in the kinetic barrier of the second dehydrogenation step of the K-doped $Mg(NH_2)_2$-2LiH system. As reported previously, KH acted catalytically to decrease the activation energy of the first dehydrogenation step of the $Mg(NH_2)_2$-2LiH-*x*KH system.[28] Moreover, it was found that the addition of Rb reduced the kinetic energy barrier of the second dehydrogenation step for the $Mg(NH_2)_2$-2LiH-*x*RbF system.[29] As a result, we believe that KH and RbH play similar catalytic roles in $Mg(NH_2)_2$-2LiH-0.04KH-0.04RbH to those in $Mg(NH_2)_2$-2LiH-*x*KH and $Mg(NH_2)_2$-2LiH-*x*RbF, respectively, because the activation energies of the first and second dehydrogenation steps of the $Mg(NH_2)_2$-2LiH-0.04KH-0.04RbH sample both decreased as mentioned above.

3.3. Changes in the Structure and Composition of $Mg(NH_2)_2$-2LiH-0.04KH-0.04RbH upon Dehydrogenation. Figure 5 shows the XRD patterns of the dehydrogenated $Mg(NH_2)_2$-2LiH-0.04KH-0.04RbH samples at different stages. As reported previously, KH and RbH phases could not be detected in the XRD profiles of the postmilled K- and Rb-doped $Mg(NH_2)_2$-2LiH samples because of their amorphization, caused by strong collisions during ball milling.[28,29]

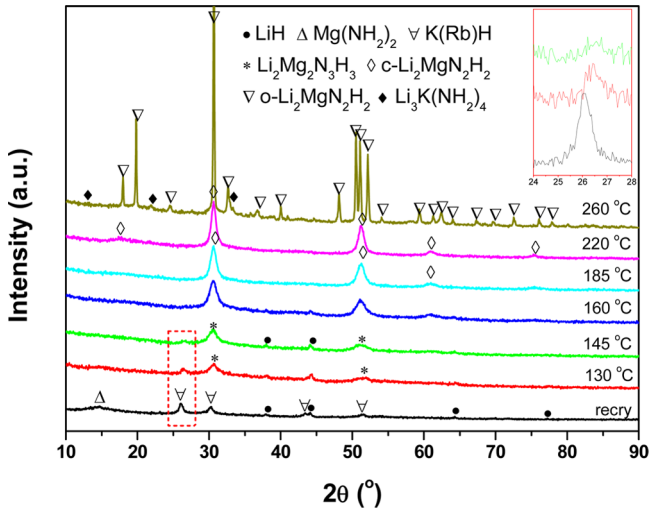

Figure 5. XRD patterns of dehydrogenated $Mg(NH_2)_2$-2LiH-0.04KH-0.04RbH samples at different stages.

Therefore, to identify the KH and RbH phases, the postmilled $Mg(NH_2)_2$-2LiH-0.04KH-0.04RbH sample was first recrystallized at 120 °C under 80 bar of H_2 pressure for 12 h. After recrystallization, four new peaks at 26.1, 30.2, 43.4, and 51.5° were observed in the XRD profile, in addition to the characteristic reflections of LiH and $Mg(NH_2)_2$, as shown in Figure 5. These four reflections resemble those of KH. However, a low-angle shift was found by carefully comparing the data with the standard pattern of KH (see Figure S2 in the Supporting Information), indicating enlarged lattice parameters. This shift is possibly due to the formation of a K(Rb)H solid solution during ball milling. It is well-known that the atomic radius of Rb (2.98 Å) is distinctly larger than that of K (2.77 Å). Consequently, the lattice parameters of a K(Rb)H solid solution should be larger than those of KH. This conjecture was verified by directly ball milling the KH-RbH mixtures. As shown in Figure S2 (see the Supporting Information), after ball milling the KH-*x*RbH mixtures, the characteristic diffraction peaks of RbH were invisible, and the diffraction peaks of KH gradually shifted to lower angles with increasing amounts of RbH. FTIR examination revealed that only the typical doublet N−H vibration of $Mg(NH_2)_2$ at 3271/3325 cm^{-1} was discernible for the recrystallized sample (Figure 6), confirming the existence of $Mg(NH_2)_2$.

After dehydrogenation at 130 °C, the diffraction peaks of the K(Rb)H solid solution were distinctly reduced and shifted to higher angles. The strongest diffraction peak of the K(Rb)H solid solution shifted from 26.1 to 26.5°, as shown in the inset of Figure 5, which is close to the standard position of a diffraction peak of KH and not RbH. This fact suggests that RbH was gradually segregated from the K(Rb)H solid solution at elevated temperatures and participated during the dehydrogenation reaction. It was reported previously that RbH could react with $Mg(NH_2)_2$ to release hydrogen and form an amide-imide complex $RbMg(NH)(NH_2)$ below 165 °C.[29] At the same time, two diffraction peaks centered at 30.7 and 51.9° were also detected in addition to those of LiH at 37.9, 44.2, and 64.7°. In particular, the peak at 51.9° is quite asymmetric, which can be resolved into two peaks at 50.7 and 52.1°, corresponding to the characteristic reflections of the tetragonal $Li_2Mg_2N_3H_3$.[32] Moreover, in addition to the characteristic N−H vibration of $Mg(NH_2)_2$ at 3271/3325 cm^{-1}, there is an new absorbance

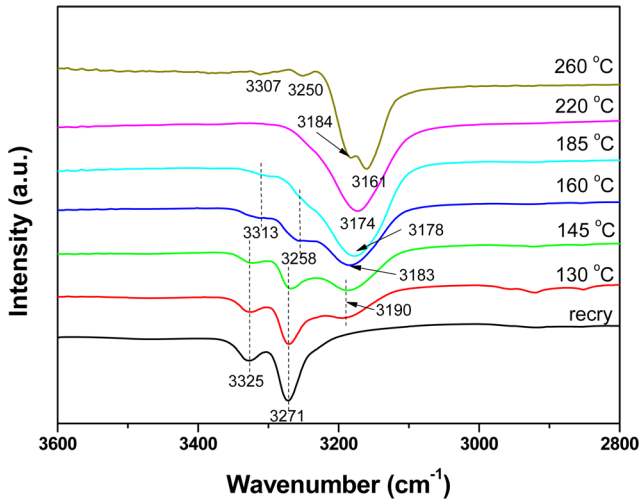

Figure 6. FTIR spectra of dehydrogenated $Mg(NH_2)_2$-2LiH-0.04KH-0.04RbH samples at different stages.

peak at 3190 cm^{-1} in the FTIR spectrum (Figure 6) that could be assigned to the N−H vibration of $Li_2Mg_2N_3H_3$.[32] After further heating of the sample to 160 °C, the diffraction peaks centered at 30.7 and 51.9° slightly moved to 30.6 and 51.3 °C and gradually intensified and changed to be symmetric along with the weakening of those of LiH and KH. Specifically, the FTIR results showed that the absorbance at 3190 cm^{-1} was distinctly intensified and moved to lower wavenumber (3183 cm^{-1}), which is closer to cubic $Li_2MgN_2H_2$. Meanwhile, a doublet absorbance at 3313/3258 cm^{-1} that can be assigned to the N−H vibration of $LiNH_2$ was detected while those of $Mg(NH_2)_2$ disappeared. It is therefore believed that the chemical reaction between $Mg(NH_2)_2$ and LiH also took place to release additional hydrogen and yield $Li_2Mg_2N_3H_3$ and $LiNH_2$ as a parallel reaction because of the catalysis of KH upon heating the sample to 160 °C.[28] Based on the previous reports,[28,29] the overall reaction process occurring below 160 °C can be written as follows.

$$2Mg(NH_2)_2 + 1.5LiH + RbH \rightarrow 0.5Li_2Mg_2N_3H_3 + 0.5LiNH_2 + RbMg(NH)(NH_2) + 2.5H_2 \quad (2)$$

When the sample was heated from 160 to 220 °C, five diffraction peaks at 17.5, 30.5, 51.2, 60.9, and 75.4° were

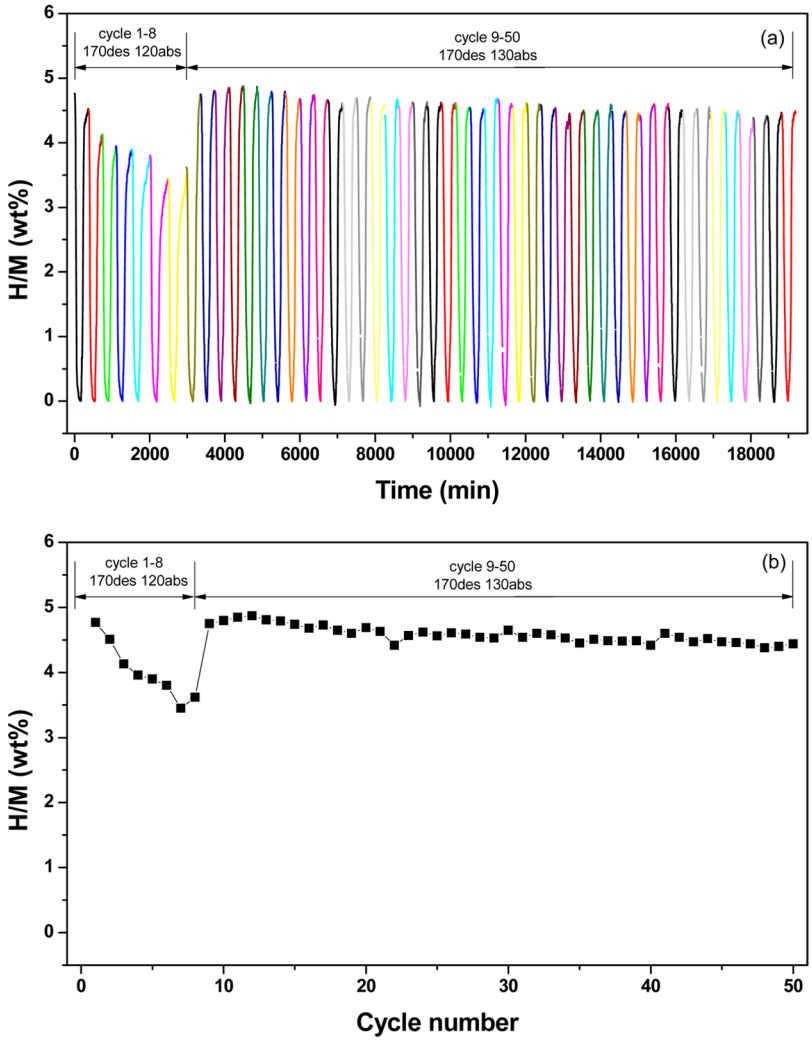

Figure 7. (a) Hydrogen desorption/absorption curves and (b) cycling capacities for reversible hydrogen storage of an $Mg(NH_2)_2$-2LiH-0.04KH-0.04RbH sample.

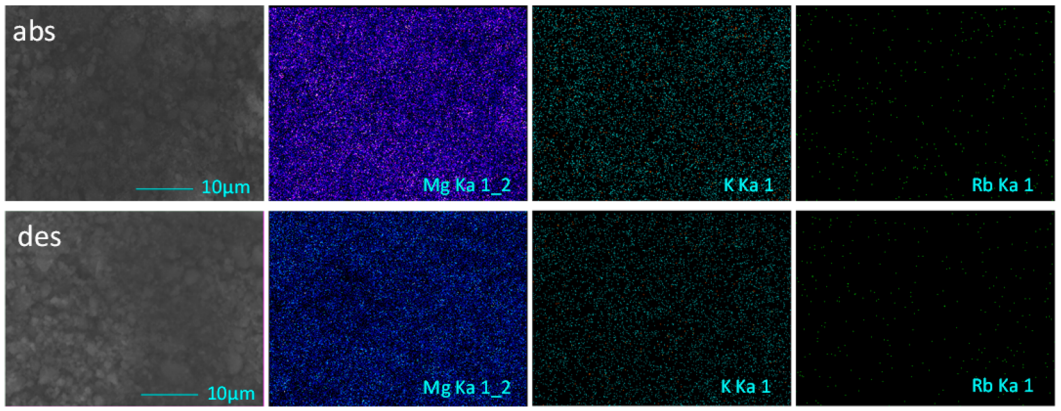

Figure 8. SEM images and EDS element maps of Mg, K and Rb for $Mg(NH_2)_2$-2LiH-0.04KH-0.04RbH samples after 50 hydrogenation/dehydrogenation cycles.

observed with considerable intensities and good symmetry in the XRD profile (Figure 5), which are consistent with the cubic $Li_2MgN_2H_2$ as reported previously.[28] At the same time, the diffraction peaks of LiH and KH were invisible, indicating that they have been consumed. According to our previous report,[28] KH reacts with $LiNH_2$, $Li_2Mg_2N_3H_3$ and LiH to convert to $Li_2MgN_2H_2$, $Li_3K(NH_2)_4$, Li_2NH, and Mg_3N_2 above 170 °C.

$$LiNH_2 + Li_2Mg_2N_3H_3 + 0.84LiH + 0.16KH \rightarrow 1.04Li_2MgN_2H_2 + 0.16Li_3K(NH_2)_4 + 0.64Li_2NH + 0.32Mg_3N_2 + H_2 \quad (3)$$

The FTIR spectrum exhibited only a broad and strong absorbance centered at 3174 cm^{-1} with the disappearance of $LiNH_2$, providing more evidence for the formation of cubic $Li_2MgN_2H_2$. After full dehydrogenation at 260 °C, reflections corresponding to orthorhombic $Li_2MgN_2H_2$ were unambiguously identified with considerable intensities in the XRD profile, while the peaks of cubic $Li_2MgN_2H_2$ nearly disappeared. Therefore, we believe that a polymorphic transformation from a cubic structure to an orthorhombic structure occurred for $Li_2MgN_2H_2$ at 220−260 °C, which corresponds to the exothermic peak in the DSC curve shown in Figure 4a.[28,29] Concurrently, the reflections of Li−K mixed amide $Li_3K(NH_2)_4$ were identified at 12.5, 21.7, and 33.3°,[28] although their intensities are quite weak. Moreover, the characteristic doublet vibration of orthorhombic $Li_2MgN_2H_2$ at 3161/3184 cm^{-1} dominated the FTIR spectrum. Meanwhile, a new doublet N−H vibration at 3250/3307 cm^{-1} was also developed, which is very similar to the characteristic absorption peaks of $Li_3K(NH_2)_4$ and $RbMg(NH)(NH_2)$.[28,29] High-resolution XPS spectra of K 2p and Rb 3d demonstrated that both K and Rb were in the +1 oxidation state in all of the dehydrogenation samples because the $2p_{3/2}$-$2p_{1/2}$ spin−orbit doublet of K appear at approximately 292.4 and 295.2 eV and the Rb 3d binding energy is approximate 110.0 eV (see Figure S3 in the Supporting Information).[33] A closer observation revealed that the binding energies of K 2p initially remained unchanged below 160 °C and then slightly increased in the range 160−260 °C. In contrast, the Rb 3d binding energy first increased and then remained constant during dehydrogenation. The high-energy shift of K 2p and Rb 3d represents the loss of electron density, indicating that K and Rb potentially bond with stronger electron-accepting elements than H with dehydrogenation,[34] which is consistent with the XRD and FTIR results. These facts confirm that the added K and Rb participate in the different dehydrogenation processes of $Mg(NH_2)_2$-2LiH system upon heating, which provides synergetic effects that improve the hydrogen storage thermodynamics and kinetics.

On the basis of the above discussion, the chemical processes during ball milling and the thermal dehydrogenation of an $Mg(NH_2)_2$-2LiH-0.04KH-0.04RbH mixture can be summarized. During ball milling, the added RbH reacted with KH to form a K(Rb)H solid solution. Upon heating, RbH first segregated from the K(Rb)H solid solution and reacted with $Mg(NH_2)_2$ to release hydrogen and generate $RbMg(NH)(NH_2)$. Concurrently, with the catalysis of KH, the chemical reaction between $Mg(NH_2)_2$ and LiH to produce $Li_2Mg_2N_3H_3$, $LiNH_2$ and H_2. This dehydrogenation process is responsible for the first endothermic peak shown in the DSC curve (Figure 4a). Then, the remaining KH and LiH reacted with the newly developed $Li_2Mg_2N_3H_3$ and $LiNH_2$ to release residual hydrogen as previously reported,[28] which corresponds to the second endothermic peak in the DSC curve. Thus, RbH and KH participated in the dehydrogenation reaction of the $Mg(NH_2)_2$-2LiH system one after the other and provided synergetic effects on improving thermodynamics and kinetics of hydrogen storage in $Mg(NH_2)_2$-2LiH system, which is the most important reason for the decreased operating temperatures and improved reaction kinetics for hydrogen storage in the $Mg(NH_2)_2$-2LiH system.

3.4. Cycling Hydrogen Storage Properties and Mechanisms of $Mg(NH_2)_2$-2LiH-0.04KH-0.04RbH. Figure 7 shows the cycling dehydrogenation/hydrogenation curves of the $Mg(NH_2)_2$-2LiH-0.04KH-0.04RbH system. To avoid the high-temperature failure of KH and RbH and maximize the hydrogen capacity,[35] the cycling measurements were performed at 170 °C/2 h for dehydrogenation and 120−130 °C/105 bar/2 h for hydrogenation. For the first 8 cycles, the hydrogenation temperature was set at 120 °C. As shown in Figure 7a, approximately 4.77 wt % of H_2 was released from the as-milled $Mg(NH_2)_2$-2LiH-0.04KH-0.04RbH sample, and the dehydrogenated product absorbed only 4.51 wt % H_2 when the dehydrogenation operated at 170 °C/2 h and the hydrogenation was at 120 °C/105 bar/2 h. This capacity is lower than the total reversible hydrogen capacity of 5.2 wt % shown in Figures 2a and 3a, possibly because of insufficient dwelling time at the corresponding operating temperatures. After 8 dehydrogenation/hydrogenation cycles, the hydrogen uptake

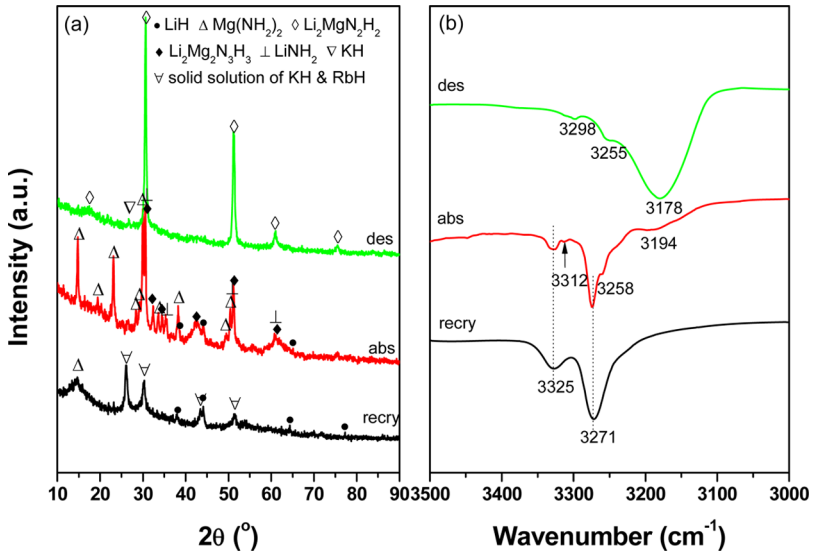

Figure 9. (a) XRD patterns and (b) FTIR spectra of the $Mg(NH_2)_2$-2LiH-0.04KH-0.04RbH samples after 50 hydrogenation/dehydrogenation cycles.

capacity was rapidly reduced to 3.62 wt % because of insufficient hydrogenation under the present conditions. To alleviate the effects of insufficient hydrogenation, the operating temperature for hydrogenation was increased to 130 °C in the following hydrogen uptake cycles. As a result, the hydrogen uptake amount increased to 4.75 wt % (Figure 7b). It can be observed that the hydrogen storage capacity stayed at 4.44 wt % after 50 cycles, which corresponds to a capacity retention of 93%. The degradation rate was determined to be only 0.0066 wt % per cycle, demonstrating markedly superior cycling stability compared with the $Mg(NH_2)_2$-2LiH and $Mg(NH_2)_2$-2LiH-0.08KH samples.[28,36]

Figure 8 shows SEM images and the EDS maps for Mg, K, and Rb of the $Mg(NH_2)_2$-2LiH-0.04KH-0.04RbH samples after 50 hydrogenation/dehydrogenation cycles. It can be observed that in both the dehydrogenation and hydrogenation cycles, the distributions of Mg, K and Rb were homogeneous, and no apparent segregation was observed. Thus, the active species of KH and RbH remained well dispersed in the Li−Mg−N−H matrix, which is likely one of the most important reasons for the persistence of their positive effects during cycling.

Figure 9 shows the XRD patterns and FTIR spectra of $Mg(NH_2)_2$-2LiH-0.04KH-0.04RbH samples after 50 cycles. As shown in Figure 9a, the sample collected in a hydrogenation cycle consisted primarily of LiH and $Mg(NH_2)_2$. Moreover, the typical N−H vibration doublet of $Mg(NH_2)_2$ at 3271/3325 cm^{-1} was discernible in the FTIR spectrum (Figure 9b). At the same time, $LiNH_2$ and $Li_2Mg_2N_3H_3$ were also identified using XRD and FTIR analyses, indicating insufficient hydrogenation. This result may explain the decreased reversible capacity after 50 cycles. For the dehydrogenation sample, the characteristic diffraction peaks of cubic $Li_2MgN_2H_2$ were unambiguously detected using XRD and FTIR. In addition, two other vibrations at 3255 and 3298 cm^{-1} were present in the FTIR spectrum, also indicating insufficient dehydrogenation. Thus, it appears that unsaturated hydrogenation remains an important reason for the decreased hydrogen capacity after 50 cycles. This conjecture was verified by increasing the hydrogenation operating temperature to 140 °C. As shown in Figure 10, approximately 4.9 wt % H_2 was desorbed from the hydrogenated 50-cycle sample at 140 °C under 105 bar of hydrogen pressure. Thus, to maintain the high hydrogen storage capacity during cycling, it is critical to appropriately adjust the operating conditions for dehydrogenation/hydrogenation.

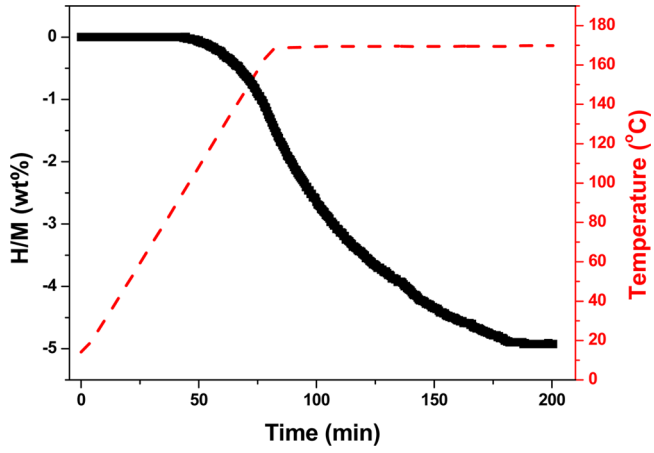

Figure 10. Volumetric release curve for an $Mg(NH_2)_2$-2LiH-0.04KH-0.04RbH sample after 50 hydrogenation/dehydrogenation cycles and hydrogenation at 140 °C.

4. CONCLUSION

In this work, KH and RbH were simultaneously introduced into the $Mg(NH_2)_2$-2LiH system to further improve its hydrogen storage properties. $Mg(NH_2)_2$-2LiH-(0.08-x)KH-xRbH (x = 0, 0.02, 0.04, 0.06, and 0.08) samples were prepared by ball milling the corresponding chemicals under 50 bar of H_2, and their dehydrogenation/hydrogenation behaviors were systematically investigated. It was found that the $Mg(NH_2)_2$-2LiH-0.04KH-0.04RbH formulation could reversibly store 5.2 wt % H_2 using a two-step reaction where the desorption operated at 130 °C and the absorption operated at 120 °C. The dehydrogenation enthalpy changes for the two steps of dehydrogenation of the $Mg(NH_2)_2$-2LiH-0.04KH-0.04RbH sample were calculated to be 38.1 ± 0.4 and 38.4 ± 0.4 kJ/mol-H_2, and the corresponding activation energies were determined to be 85.6 ± 4.5 kJ/mol and 98.1 ± 2.4 kJ/mol,

dx.doi.org/10.1021/am504592x | ACS Appl. Mater. Interfaces 2014, 6, 17024−17033

which were lower than those of the pristine sample. Structural analysis revealed that KH first reacted with RbH to generate a K(Rb)H solid solution during ball milling. Upon heating, RbH separated from the K(Rb)H solid solution and reacted with $Mg(NH_2)_2$ to release hydrogen and generate $RbMg(NH)(NH_2)$. Concurrently, with the catalysis of KH, the chemical reaction between $Mg(NH_2)_2$ and LiH occurred to produce $Li_2Mg_2N_3H_3$, $LiNH_2$, and H_2. Then, the remaining KH and LiH reacted with the newly developed $Li_2Mg_2N_3H_3$ and $LiNH_2$ to release the residual hydrogen associated with the catalysis of $RbMg(NH)(NH_2)$. Thus, RbH and KH combined to provide synergetic effects, improving the thermodynamics and kinetics of hydrogen storage in the $Mg(NH_2)_2$-2LiH system. While operating at 170 °C/2 h for dehydrogenation and 130 °C/2 h for hydrogenation, the hydrogen capacity of the $Mg(NH_2)_2$-2LiH-0.04KH-0.04RbH sample remained as high as 4.44 wt % after 50 cycles, corresponding to a capacity retention ratio of 93%. This stability was superior to that of the pristine $Mg(NH_2)_2$-2LiH and KH-modified samples.

■ ASSOCIATED CONTENT

Supporting Information

Dehydrogenation/hydrogenation curves of $Mg(NH_2)_2$-2LiH-0.04RbH and $Mg(NH_2)_2$-2LiH-0.04KH-0.04RbH, XRD patterns of KH-*x*RbH, High-resolution XPS spectra of K 2p and Rb 3d. This material is available free of charge via the Internet at http://pubs.acs.org.

■ AUTHOR INFORMATION

Corresponding Author

*E-mail: mselyf@zju.edu.cn. Tel/Fax: +86 571 87952615.

Notes

The authors declare no competing financial interest.

■ ACKNOWLEDGMENTS

The authors acknowledge financial support from the Ministry of Science and Technology of China (2010CB631304), the National Natural Science Foundation of China (51222101, 51025102, 51171170), the Research Fund for the Doctoral Program of Higher Education of China (20130101110080, 20130101130007), the Program for Innovative Research Team in University of Ministry of Education of China (IRT13037), and the Science and Technology Department of Zhejiang Province (2010R50013).

■ REFERENCES

(1) Schlapbach, L.; Zuttel, A. Hydrogen-storage Materials for Mobile Applications. *Nature* **2001**, *414*, 353−358.
(2) Züttel, A. Hydrogen Storage Methods. *Naturwissenschaften* **2004**, *91*, 157−172.
(3) Chen, P.; Zhu, M. Recent Progress in Hydrogen Storage. *Mater. Today* **2008**, *11*, 36−43.
(4) Kelly, M. T. Perspective on the Storage of Hydrogen: Past and Future. *Struct. Bonding (Berlin)* **2011**, *141*, 169−201.
(5) Durbin, D. J.; Malardier-Jugroot, C. Review of Hydrogen Storage Techniques for on Board Vehicle Applications. *Int. J. Hydrogen Energy* **2013**, *38*, 14595−14617.
(6) Targets for Onboard Hydrogen Storage Systems for Light-Duty Vehicles, US DOE EB/OL. https://www1eereenergygov/hydrogenandfuelcells/storage/pdfs/targets_onboard_hydro_storage_explanationpdf. Accessed 10 October 2009.
(7) Jena, P. Materials for Hydrogen Storage: Past, Present, and Future. *J. Phys. Chem. Lett.* **2011**, *2*, 206−211.
(8) Bogdanović, B.; Schwickardi, M. Ti-doped Alkali Metal Aluminium Hydrides as Potential Novel Reversible Hydrogen Storage Materials. *J. Alloys Compd.* **1997**, *253*−*254*, 1−9.
(9) Pang, Y. P.; Liu, Y. F.; Gao, M. X.; Ouyang, L. Z.; Liu, J. W.; Wang, H.; Zhu, M.; Pan, H. G. A Mechanical-force-driven Physical Vapour Deposition Approach to Fabricating Complex Hydride Nanostructures. *Nat. Commun.* **2014**, *5*, 3519.
(10) Liang, C.; Liu, Y. F.; Fu, H. L.; Ding, Y. F.; Gao, M. X.; Pan, H. G. Li-Mg-N-H-based Combination Systems for Hydrogen Storage. *J. Alloys Compd.* **2011**, *509*, 7844−7853.
(11) Xiong, Z. T.; Wu, G. T.; Hu, H. J.; Chen, P. Ternary Imides for Hydrogen Storage. *Adv. Mater.* **2004**, *16*, 1522−1525.
(12) Luo, W. F. ($LiNH_2$-MgH_2): a Viable Hydrogen Storage System. *J. Alloys Compd.* **2004**, *381*, 284−287.
(13) Xiong, Z. T.; Hu, J. J.; Wu, G. T.; Chen, P.; Luo, W. F.; Gross, K.; Wang, J. Thermodynamic and Kinetic Investigations of the Hydrogen Storage in the Li-Mg-N-H System. *J. Alloys Compd.* **2005**, *398*, 235−239.
(14) Sudik, A.; Yang, J.; Halliday, D.; Wolverton, C. Kinetic Improvement in the $Mg(NH_2)_2$-LiH Storage System by Product Seeding. *J. Phys. Chem. C* **2007**, *111*, 6568−6573.
(15) Xie, L.; Liu, Y.; Li, G. Q.; Li, X. G. Improving Hydrogen Sorption Kinetics of the $Mg(NH_2)_2$-LiH System by the Tuning Particle Size of the Amide. *J. Phys. Chem. C* **2009**, *113*, 14523−14527.
(16) Liu, Y. F.; Zhong, K.; Luo, K.; Gao, M. X.; Pan, H. G.; Wang, Q. D. Size-Dependent Kinetic Enhancement in Hydrogen Absorption and Desorption of the Li-Mg-N-H System. *J. Am. Chem. Soc.* **2009**, *131*, 1862−1870.
(17) Chen, Y.; Wang, P.; Liu, C.; Cheng, H. M. Improved Hydrogen Storage Performance of Li-Mg-N-H Materials by Optimizing Composition and Adding Single-walled Carbon Nanotubes. *Int. J. Hydrogen Energy* **2007**, *32*, 1262−1268.
(18) Lohstroh, W.; Fichtner, M. Reaction Steps in the Li-Mg-N-H Hydrogen Storage System. *J. Alloys Compd.* **2007**, *446*, 332−335.
(19) Shahi, R. R.; Yadav, T. P.; Shaz, M. A.; Srivastva, O. N. Studies on Dehydrogenation Characteristic of $Mg(NH_2)_2$/LiH Mixture Admixed with Vanadium and Vanadium Based Catalysts (V, V_2O_5 and VCl_3). *Int. J. Hydrogen Energy* **2010**, *35*, 238−246.
(20) Ma, L. P.; Dai, H. B.; Liang, Y.; Kang, X. D.; Fang, Z. Z.; Wang, P. J.; Wang, P.; Cheng, H. M. Catalytically Enhanced Hydrogen Storage Properties of $Mg(NH_2)_2$+2LiH Material by Graphite-Supported Ru Nanoparticles. *J. Phys. Chem. C* **2008**, *112*, 18280−18285.
(21) Hu, J. J.; Liu, Y. F.; Wu, G. T.; Xiong, Z. T.; Chua, Y. S.; Chen, P. Improvement of Hydrogen Storage Properties of the Li-Mg-N-H System by Addition of $LiBH_4$. *Chem. Mater.* **2008**, *20*, 4398−4402.
(22) Hu, J. J.; Pohl, A.; Wang, S. M.; Rothe, J.; Fichtner, M. Additive Effects of $LiBH_4$ and $ZrCoH_3$ on the Hydrogen Sorption of the Li-Mg-N-H Hydrogen Storage System. *J. Phys. Chem. C* **2012**, *116*, 20246−20253.
(23) Li, B.; Liu, Y. F.; Gu, J.; Gao, M. X.; Pan, H. G. Synergetic Effects of In Situ Formed CaH_2 and $LiBH_4$ on Hydrogen Storage Properties of the Li-Mg-N-H System. *Chem.—Asian J.* **2013**, *8*, 374−384.
(24) Liu, Y. F.; Hu, J. J.; Xiong, Z. T.; Wu, G. T.; Chen, P. Improvemient of the Hydrogen-storage Performances of Li-Mg-N-H System. *J. Mater. Res.* **2007**, *22*, 1339−1345.
(25) Wang, J. H.; Liu, T.; Wu, G. T.; Li, W.; Liu, Y. F.; Araujo, C. M.; Scheicher, R. H.; Blomqvist, A.; Ahuja, R.; Xiong, Z. T.; Yang, P.; Gao, M. X.; Pan, H. G.; Chen, P. Potassium-Modified $Mg(NH_2)_2$/2LiH System for Hydrogen Storage. *Angew. Chem., Int. Ed.* **2009**, *48*, 5828−5832.
(26) Luo, W.; Stavila, V.; Klebanoff, L. E. New Insights into the Mechanism of Activation and Hydrogen Absorption of ($2LiNH_2$-MgH_2). *Int. J. Hydrogen Energy* **2012**, *37*, 6646−6652.
(27) Durojaiye, T.; Goudy, A. Desorption Kinetics of Lithium Amide/Magnesium Hydride Systems at Constant Pressure Thermodynamic Driving Forces. *Int. J. Hydrogen Energy* **2012**, *37*, 3298−3304.

(28) Li, C.; Liu, Y. F.; Pang, Y. P.; Gu, Y. J.; Gao, M. X.; Pan, H. G. Compositional Effects on the Hydrogen Storage Properties of $Mg(NH_2)_2$-2LiH-xKH and the Activity of KH During Dehydrogenation Reactions. *Dalton Trans.* **2014**, *43*, 2369−2377.
(29) Li, C.; Liu, Y. F.; Gu, Y. J.; Gao, M. X.; Pan, H. G. Improved Hydrogen-Storage Thermodynamics and Kinetics for an RbF-Doped $Mg(NH_2)_2$-2LiH System. *Chem.—Asian J.* **2013**, *8*, 2136−43.
(30) Durojaiye, T.; Hayes, J.; Goudy, A. Rubidium Hydride: An Exceptional Dehydrogenation Catalyst for the Lithium Amide/Magnesium Hydride System. *J. Phys. Chem. C* **2013**, *117*, 6554−6560.
(31) Kissinger, H. E. Reaction Kinetics In Differential Thermal Analysis. *Anal. Chem.* **1957**, *29*, 1702−1706.
(32) Hu, J. J.; Liu, Y. F.; Wu, G. T.; Xiong, Z. T.; Chen, P. Structural and compositional changes during hydrogenation/dehydrogenation of the Li-Mg-N-H system. *J. Phys. Chem. C* **2007**, *111*, 18439−18443.
(33) Morgan, W. E.; Van Wazer, J. R.; Stec, W. J. Inner-Orbital Photoelectron Spectroscopy Of Alkali-Metal Halides, Perchlorates, Phosphates, And Pyrophosphates. *J. Am. Chem. Soc.* **1973**, *95*, 751−755.
(34) Chae, I. S.; Kim, M.; Kang, Y. S.; Kang, S. W. Enhanced CO2 carrier activity of potassium cation with fluorosilicate anions for facilitated transport membranes. *J. Membr. Sci.* **2014**, *466*, 357−360.
(35) Li, C.; Liu, Y. F.; Yang, Y. J.; Gao, M. X.; Pan, H. G. High-temperature Failure Behaviour and Mechanism of K-based Additives in Li-Mg-N-H Hydrogen Storage Systems. *J. Mater. Chem. A* **2014**, *2*, 7345−7353.
(36) Luo, W. F.; Wang, J.; Stewart, K.; Clift, M.; Gross, K. Li-Mg-N-H: Recent Investigations and Development. *J. Alloys Compd.* **2007**, *446*, 336−341.